Fundus Autofluorescence Findings in a Mouse Model of Retinal Detachment

Roberta Secondi,[1,2] *Jian Kong,*[1] *Anna M. Blonska,*[1] *Giovanni Staurenghi,*[2] *and Janet R. Sparrow*[1,3]

Purpose. Fundus autofluorescence (fundus AF) changes were monitored in a mouse model of retinal detachment (RD).

Methods. RD was induced by transscleral injection of hyaluronic acid (Healon) or sterile balanced salt solution (BSS) into the subretinal space of 4–5-day-old albino *Abca4* null mutant and *Abca4* wild-type mice. Images acquired by confocal scanning laser ophthalmoscopy (Spectralis HRA) were correlated with spectral domain optical coherence tomography (SD-OCT), infrared reflectance (IR), fluorescence spectroscopy, and histologic analysis.

Results. In the area of detached retina, multiple hyperreflective spots in IR images corresponded to punctate areas of intense autofluorescence visible in fundus AF mode. The puncta exhibited changes in fluorescence intensity with time. SD-OCT disclosed undulations of the neural retina and hyperreflectivity of the photoreceptor layer that likely corresponded to histologically visible photoreceptor cell rosettes. Fluorescence emission spectra generated using flat-mounted retina, and 488 and 561 nm excitation, were similar to that of RPE lipofuscin. With increased excitation wavelength, the emission maximum shifted towards longer wavelengths, a characteristic typical of fundus autofluorescence.

Conclusions. In detached retinas, hyper-autofluorescent spots appeared to originate from photoreceptor outer segments that were arranged within retinal folds and rosettes. Consistent with this interpretation is the finding that the autofluorescence was spectroscopically similar to the bisretinoids that constitute RPE lipofuscin. Under the conditions of a RD, abnormal autofluorescence may arise from excessive production of bisretinoid by impaired photoreceptor cells. (*Invest Ophthalmol Vis Sci.* 2012;53:5190–5197) DOI:10.1167/iovs.12-9672

Retinal detachment (RD) results in the loss of apposition between the neural retina and the underlying RPE cell layer. Previous studies in human and animal retinas have demonstrated that RD induces a complex cascade of events leading to photoreceptor cell degeneration, and RD-associated vision loss.[1] Animal models of RD have been studied previously by funduscopy, optical coherence tomography (OCT) and histologic analyses.[2–4] Using these modalities, studies have documented various structural changes within detached retina, including abnormalities of photoreceptor outer segments (OS) and thinning of the outer nuclear layer (ONL).[5,6]

To the best of our knowledge, studies thus far have not examined RDs by fundus autofluorescence (AF). Fundus AF is a modality that relies primarily on the fluorescence generated from the bisretinoids of lipofuscin in retinal pigment epithelial cells.[7] These bisretinoid compounds form in photoreceptor cells from reaction of vitamin A aldehyde, the latter being generated as a consequence of the cells' light capturing function. The bisretinoids subsequently are transferred to RPE during the process of photoreceptor outer segment membrane shedding and phagocytosis.[8] Elevated fundus autofluorescence, caused by abnormal accumulations of RPE bisretinoids often are noticed in retinal disorders, such as recessive Stargardt disease,[9] dominant Stargardt-like macular degeneration,[10] and in Best vitelliform macular dystrophy.[11] Factors that can contribute to fundus hyperfluorescence in other forms of retinal degenerations, including age-related macular degeneration (AMD) and retinitis pigmentosa (RP), also have been studied.[12–14]

Fundus autofluorescence in the presence of a serous RD in humans recently has attracted attention.[15–17] Efforts to determine the origin of fundus autofluorescence patterns in central serous chorioretinopathy, and to correlate fundus AF with ophthalmoscopic and SD-OCT findings have led to the suggestion that in the presence of a serous detachment, autofluorescence originates from elongated photoreceptor outer segments that are not phagocytized by the RPE due to loss of photoreceptor-RPE apposition.[17] We have hypothesized that augmented fundus autofluorescence in retinal disease can originate abnormally from accelerated bisretinoid formation in impaired photoreceptor cells.[18]

Our current study was done to examine fundus autofluorescence changes in a mouse model of RD. To this end, we acquired fundus AF images using a confocal scanning laser ophthalmoscope (Spectralis HRA; Heidelberg Engineering, Heidelberg, Germany) equipped with an internal AF reference.[19] To optimize the sensitivity of our analysis, we used the *Abca4* null mutant mouse, a model of recessive Stargardt disease that is characterized by an excessive accumulation of RPE lipofuscin.[20,21] We investigated fundus AF patterns in *Abca4* null mutant and wild-type mice under conditions of a RD, and we correlated these images with infrared reflectance, OCT, histology, and fluorescence spectroscopy.

Materials and Methods

Animals

Albino *Abca4/Abcr* null mutant mice and albino *Abca4* wild-type mice, both homozygous for Rpe65-Leu450 (female and male) were generated and genotyped.[22] Mice were housed under standard 12-hour on-off

From the Departments of [1]Ophthalmology, and [3]Pathology and Cell Biology, Columbia University, New York, New York; and the [2]Eye Clinic, Department of Clinical Science, Luigi Sacco Hospital, University of Milan, Milan, Italy.

Supported by National Institutes of Health Grants EY12951, P30EY019007, and R24 EY019861; a grant from Research to Prevent Blindness to the Department of Ophthalmology; and by funding from Luigi Sacco Hospital, University of Milan (RS).

Submitted for publication February 9, 2012; revised June 27, 2012; accepted July 1, 2012.

Disclosure: **R. Secondi**, None; **J. Kong**, None; **A.M. Blonska**, None; **G. Staurenghi**, None; **J.R. Sparrow**, None

Corresponding author: Janet R. Sparrow, Columbia University, Department of Ophthalmology, 630 W. 168th Street, New York, NY 10032; jrs88@columbia.edu.

Investigative Ophthalmology & Visual Science, August 2012, Vol. 53, No. 9

cyclic lighting with in-cage illuminance of 30–80 lux. Subretinal injection, fundus autofluorescence imaging, spectral domain OCT (SD-OCT) and histologic analysis were performed in *Abca4*$^{-/-}$ and *Abca4*$^{+/+}$ mice.

RD Surgery

Abca4$^{-/-}$ ($n = 16$) and *Abca4*$^{+/+}$ ($n = 10$) mice underwent RD surgery on postnatal day 4 or 5. Surgery was performed by the same experienced operator using an operating microscope (Leica Microsystem M501, Wetzlar, Germany) to visualize the retina and to confirm the presence of the detachment. RD was created in the right eyes of mice as described previously, with minor modification.[2,23] Briefly, under hypothermia anesthesia, the eyelids were opened to proptose the eyeball and a sclerotomy was created approximately 2 mm posterior to the limbus with a 30-gauge microvitreoretinal blade (Alcon MIVS, Hünenberg, Switzerland). The tip of a small-bore (100 μm), custom-pulled glass pipette was guided into the sclera and then tangentially to enter the subretinal space in the inferotemporal quadrant. Hyaluronic acid (Healon, 10 mg/ml; AMO, Santa Ana, CA; 12 *Abca4*$^{-/-}$ and 5 *Abca4*$^{+/+}$ mice) or sterile balanced salt solution (BSS, 15 ml; Alcon, Fort Worth, TX; 4 *Abca4*$^{-/-}$ and 5 *Abca4*$^{+/+}$ mice) was injected subretinally in 1 μL volume to produce an RD that extended from approximately 8–1 o'clock clockwise, covering approximately 30–40% of the fundus. All procedures were performed in accordance with the ARVO Statement for the Use of Animals in Ophthalmic and Vision Research, and the guidelines established by the Institutional Animal Care and Use Committee (IACUC).

Fundus Autofluorescence Imaging

Using a confocal scanning laser ophthalmoscope (Spectralis HRA, Heidelberg Engineering, Heidelberg, Germany) infrared reflectance (IR) was recorded at 830 nm and fundus AF images were acquired using a 488 nm excitation wavelength. Imaging was performed on days 15, 30, 45, 60, 75, and 90 after RD was induced. For image acquisition mice were anesthetized with an intraperitoneal injection of ketamine (100 mg/kg, Ketaset; Fort Dodge Animal Health, Fort Dodge, IA) and xylazine (10 mg/kg, Anased; Lloyd Laboratories, Shenandoah, IA), and kept warm using a temperature control system. The pupils were dilated with phenylephrine hydrochloride (Mydfrin 2.5%; Alcon) and tropicamide (Mydriacyl 0.5%; Alcon). A drop of Gen Teal Liquid Gel (Novartis, East Hanover, NJ) was applied to the surface of the cornea to maintain hydration and clarity, and to prevent cataract formation. To allow appropriate positioning of the mouse, an adjustable custom-made platform was used. All images were acquired in the high-speed mode with a 55° field, digitized in frames of 768 × 768 pixels with a resolution of approximately 11 mm per pixel (8.9 frames/second), starting centrally, and extending into the mid and far periphery focusing on the temporal detached quadrant of the retina. For consistency, detector sensitivity was maintained at fixed values for all the animals and at all follow-up time points. The Spectralis was modified to house an internal fluorescence reference. The reference is visible at the top of the fundus AF images, the brightness of the reference facilitating qualitative monitoring of changes in autofluorescence.

OCT

In vivo ultra-high resolution OCT was performed using a spectral domain OCT system (Envisu R2200 VHR SDOIS, Bioptigen Inc., Durham, NC) on day 45 after RD induction. A stereotaxic alignment stage with three-dimensional free rotation about the eye center was used for mouse positioning. Images were obtained in the temporal quadrant centered on the area of maximal RD. Each high-density three-dimensional OCT volume recorded at the maximum field-of-view consisted of either 1000 A-scans per B-scan and 100 B-scans per volume or 400 A-scans per B-scan and 400 B-scans per volume. B-scans were acquired, processed, and displayed in real-time at 32 frames per second. The 3D OCT volume size was 1.6 × 1.6 mm laterally and 1.8 mm axially. Optical depth resolution in tissue was approximately 3 μm, with digital resolution reaching 1.6 μm. Measurements were made with axial and transverse on-screen digital calipers that were calibrated by the manufacturer according to a typical wild-type mouse with fixed eye dimensions.

Histology

Mouse eyes were fixed with a mixture of 4% paraformaldehyde, 16.8% isopropyl alcohol, 2% trichloroacetic acid, and 2% zinc chloride in phosphate buffer for 24 hours at 4°C. The superior pole of the eye was marked. Whole eyecups were embedded in paraffin and sectioned at a thickness of 8 μm. Sections then were counterstained using hematoxylin and eosin (H&E). Morphologic observations and light microscopy were performed using a digital imaging system (Leica Microsystems, Welzlar, Germany). Histologic analysis was guided by fundus AF images focusing on the detached quadrant of the retina. Alternatively, the posterior segment of the eye was prepared as a flat-mount that was fixed in 4% paraformaldehyde for 1 hour and mounted in Vectashield (Vector Laboratory, Burlingame, CA). Retinas were photographed immediately using a fluorescence microscope (Zeiss Laser Scan Microscopy LSM 410; Carl Zeiss Microscopy, LLC, Thornwood, NY) and a ×10 objective.

Fluorescence Spectroscopy

Fluorescence emission spectra were obtained from flat-mounted retinae of *Abca4*$^{-/-}$ mice 45 days after surgery (50 days of age). The spectra were recorded at 6 nm increments using the ×60 objective of a confocal laser scanning fluorescence microscope (Nikon A1R MP; Nikon Instruments, Inc., Melville, NY) equipped with a spectral detector, and 488 and 561 nm laser lines. Emission was collected at $\lambda_{em} \geq 500$ nm. Spectra were adjusted for pixel size and laser power. The field size was approximately 1 × 1 μm (512 × 512 pixels, 0.004 micrometers per pixel). Pixel values over fluorescent regions of interest were averaged.

Results

Changes in Fundus Infrared Reflectance and Fundus Autofluorescence

When nondetached and detached retinas were compared by IR (Figs. 1A, 1D), the area of the RD could be recognized readily as a dark region with indistinct margins. The IR images also displayed multiple hyperreflective spots within the area of the detachment (Fig. 1D); these lesions corresponded to punctate areas of intense autofluorescence found in the AF mode (Figs. 1E [circle], 1F). In fellow eyes with nondetached retinas, hyperautofluorescent spots were not observed in fundus AF images (Figs. 1B, 1C). Serial postsurgical fundus AF imaging of mice exhibiting RD revealed consistent changes in the brightness, number, and size of the spots (Fig. 2). Specifically, in fundus AF images obtained 15 days after inducing the RD, the hyperfluorescent puncta were visible in the area of detachment. Spot size in fundus AF images was approximately 185 μm (mean 10 spots, range 105–265 μm) in the RD-*Abca4*$^{-/-}$ mouse model. The hyperfluorescent spots increased gradually in brightness and number between days 30 and 45, and then faded progressively at later follow-up imaging (75 and 90 days, Fig. 2, compare areas marked by white arrows). By day 90 the fluorescence of most spots had decreased leaving an irregular and nonhomogeneous zone of AF (Fig. 2F, arrows). All mice in which RD was induced, whether *Abca4*$^{-/-}$ or *Abca4*$^{+/+}$, exhibited a characteristic pattern of granular hyperfluorescent

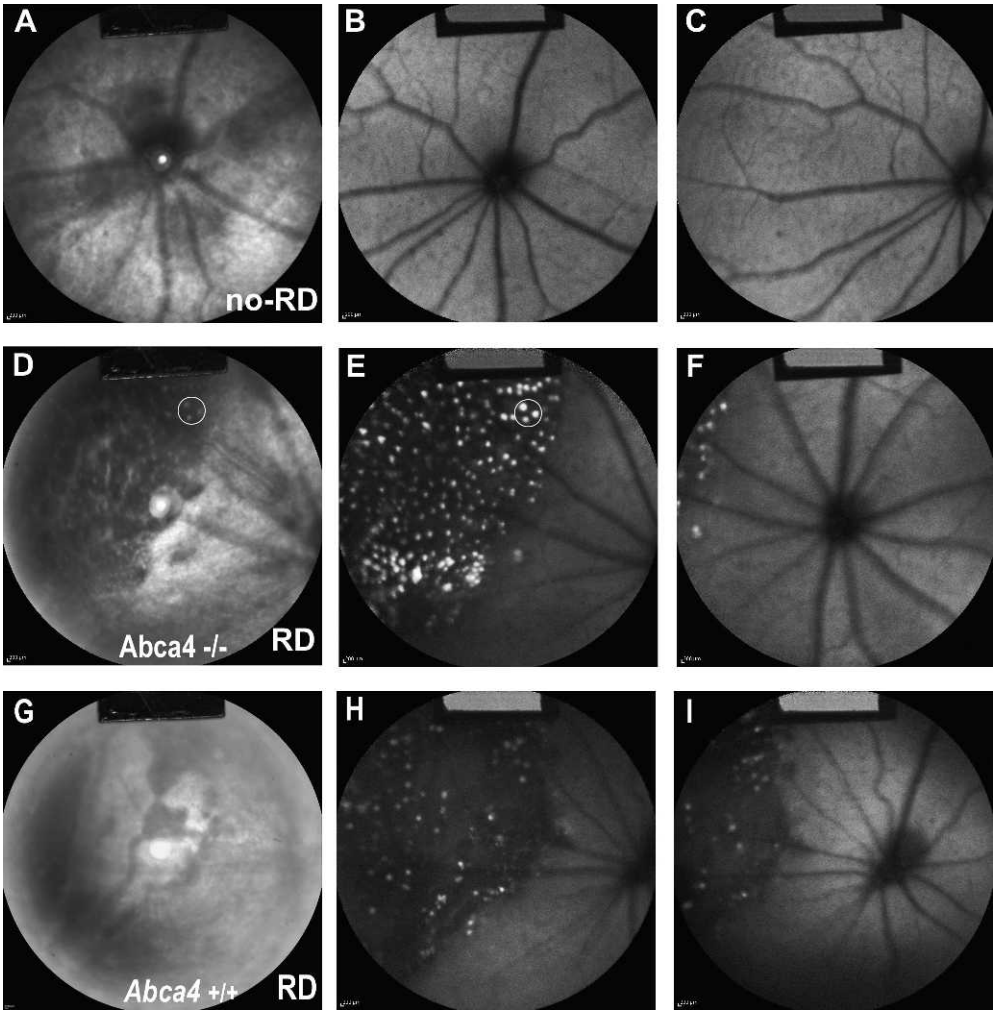

Figure 1. IR (**A**, **D**, **G**) and fundus AF (**B**, **C**, **E**, **F**, **H**, **I**) images of the no-RD (**A–C**) and RD (**D–F**) *Abca4*$^{-/-}$ eyes of the same mouse at 50 days of age, and RD (**G–I**) *Abca4*$^{+/+}$ eyes at 45 days of age. IR image (**A**) and fundus AF images (**B**, **C**) of the no-RD retina were acquired centrally (**B**) and peripherally (**C**), and reveal a homogeneous pattern with no evidence of hyper-autofluorescent spots. Fundus AF images of the detached retina show multiple hyper-autofluorescent spots in the mid-periphery (**E**, *white circle*) that correspond to hyperreflective spots within the detached retina (*darkened area*) in the IR image (**D**, *white circle*). The fundus AF image acquired centrally in the detached eye shows bright spots at the edge of the detachment (**F**). IR (**G**) and AF (**H**, **I**) images of the *Abca4*$^{+/+}$ mouse show analogous hyper-autofluorescent spots within the detached retina. An internal fluorescent reference is visible in the image (*top*). The Spectralis device used for these studies was equipped with this reference to enable quantitation of fundus fluorescence intensity.[19]

spots distributed randomly in the detached area (Figs. 1E, 1F, 1H, 1I). There were no qualitative differences in the appearance of the spots and the time over which the spots developed was similar. In both groups of mice the distribution of the spots also matched the extent of the RD. No differences also were noted when retinas were detached by subretinal injection of BSS versus Healon (not shown).

SD-OCT Imaging

SD-OCT images were taken on day 45 after RD induction; at this time the spots exhibited the greatest autofluorescence in AF mode. Images were acquired at the readily recognized transition between attached and detached retina, and in areas corresponding to the maximal height of the RD. When images were obtained within the zone of attached retina (Fig. 3A), typical bands of varying reflectivity were discernible in the OCT image, including the hyperreflective bands in outer retina attributable to the external limiting membrane (ELM), ellipsoid region of photoreceptor inner segments (IS ELLIPSOID, also referred to as inner segment/outer segment [IS/OS] junction), and bands corresponding to the contact cylinders (outer segments ensheathed by RPE microvilli) along with RPE and Bruch's membrane.[24,25] Conversely, within the detached area, retinal layers were not distinct (Figs. 3B–3D). Furthermore, where the height of the RD was maximal, the ELM and IS ellipsoid band were discontinuous or undetectable. Occasionally, hyperreflective material appeared to protrude from the detached retinal surface (Figs. 3C, 3D, white arrows; Fig. 4A, white arrows). Frequently, the normal planar organization of the neural retina gave way to abnormal undulations or semirosettes (Figs. 4A, 4D). The latter often exhibited central hyperreflective cores (Figs. 3D, 4A, 4D). The core visible in Figure 3 measured approximately 192 × 156 μm along the vertical and horizontal axes, respectively (Fig. 3D).

Ex Vivo Findings

Histologic examination was performed 45 days following the detachment. H&E-stained retinal sections from mice that

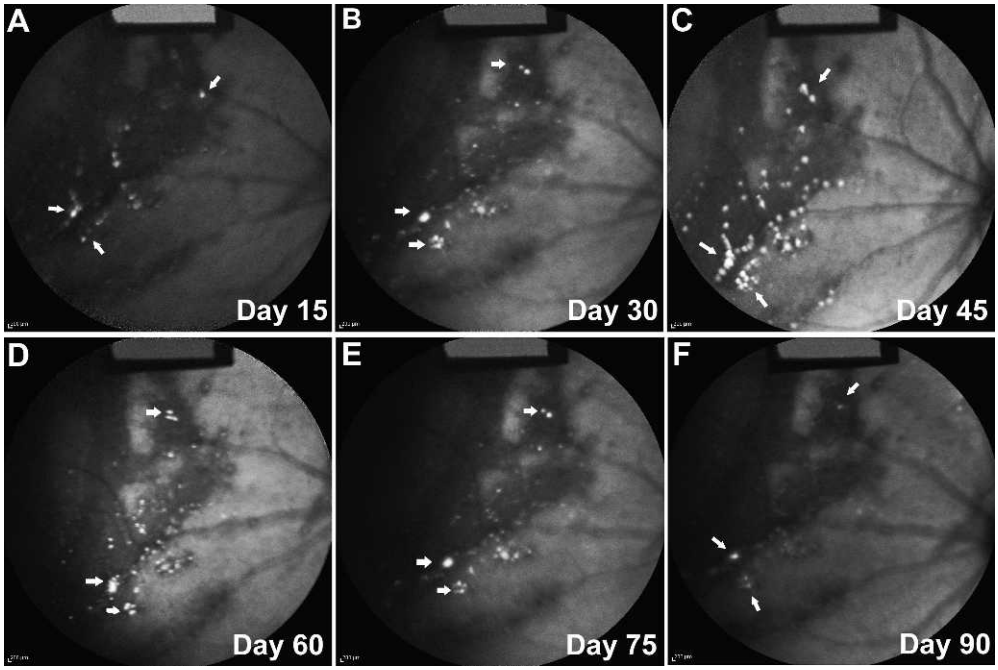

Figure 2. Fundus AF imaging of *Abca4*$^{-/-}$ mice shows that the hyperfluorescent spots changed with time post-detachment. cSLO and 488 nm excitation were used. *White arrows*: examples of changes in spot brightness and number. Fluorescence intensity and number of the spots increased between 15 (**A**) and 45 (**C**) days, and then decreased gradually at days 60 (**D**), 75 (**E**), and 90 (**F**) post-detachment. The internal reference (*top*) can assist in this qualitative assessment. Detector sensitivity was maintained at fixed values.

received subretinal injections displayed separation of the retina from the underlying RPE layer (Figs. 4B, 4C, 4E, 4F, 4H, 4I). Comparison of attached and detached areas of retina in the same eye revealed a significant asymmetry in the laminar structure. Specifically, retinal layers were distorted in the area of the detachment (Figs. 4B, 4C, 4E, 4F, 4H, 4I) while in contrast, the uninjured part of the retina appeared normal morphologically (Fig. 4G). Light micrographs also showed that the disarrangement extended into inner retina (Figs. 4B, 4E) and the latter could appear edematous (Fig. 4C). Additionally, in the area of detached retina, the ONL was thrown into folds (for instance, Figs. 4B, 4E, 4F; thick black arrows). The photoreceptor cells within the detached area of retina were rearranged and often formed abnormal rosette-like structures (Fig. 4I). Moreover the outer segments appeared to be of variable lengths (Fig. 4C, thin black arrows) compared to outer segments in attached areas of retina (Fig. 4G). Dispersed cell nuclei also were visible in the subretinal space (Figs. 4B, 4H; arrowheads). Rosette formation appeared to be developed more fully in areas in which the detachment was shallow (Fig. 4I). When fixed flat-mounted retinas were examined by fluorescence microscopy, numerous hyperfluorescent spots were visible in the area of the detachment in the RD-*Abca4*$^{-/-}$ mice (45 days post-detachment, Fig. 5B).

Fluorescence Emission Spectra

Fluorescence emission spectra were obtained from flat-mounted retinas of *Abca4*$^{-/-}$ mice 45 days after RD surgery (50 days of age, Fig. 6). As shown in the confocal microscopic images in Figure 6, fluorescence spectra were recorded from the hyper-autofluorescent puncta ("on spot;" orange spots in Fig. 6B), and from the surrounding background ("off spot;" Fig. 6C). On-spot emission spectra from RD-*Abca4*$^{-/-}$ retina exhibited fluorescence peaks at 581 and 629 nm, with excitations at 488 and 561 nm, respectively (Fig. 6A). The

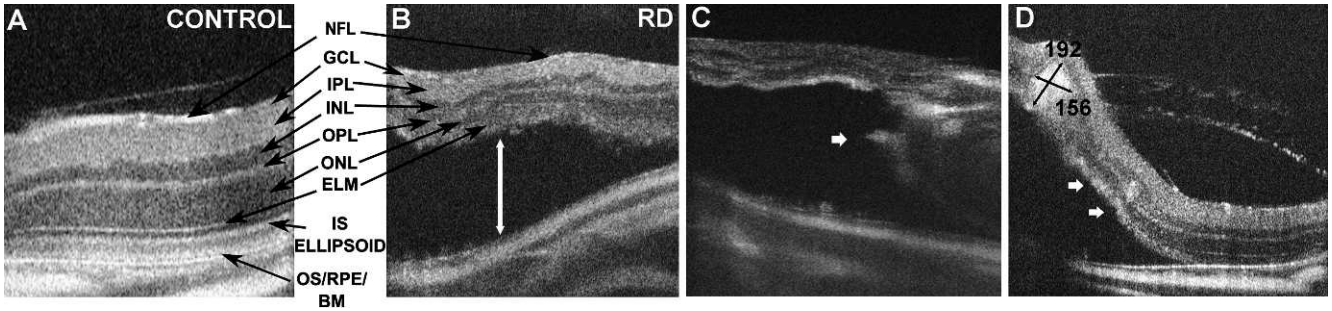

Figure 3. SD-OCT images of *Abca4*$^{-/-}$ mouse. (**A**) Normal retina of *Abca4*$^{-/-}$ mouse. Assignment of reflectivity bands is based on report of Spaide and Curcio.[25] NFL, nerve fiber layer; GCL, ganglion cell layer; IPL, inner plexiform layer; INL, inner nuclear layer (INL); OPL, outer plexiform layer; OS/RPE/BM, contact cylinders/RPE/Bruch's membrane. (**B**) Disorganized *Abca4*$^{-/-}$ retina 45 days after detachment. *White arrow* indicates the subretinal space in the area of detachment. (**C**, **D**) *Short white arrows* point to hyperreflectivity on outer retinal face of the detachment. Optical spot size of hyperreflective core in (**D**) is 192 × 156 μm.

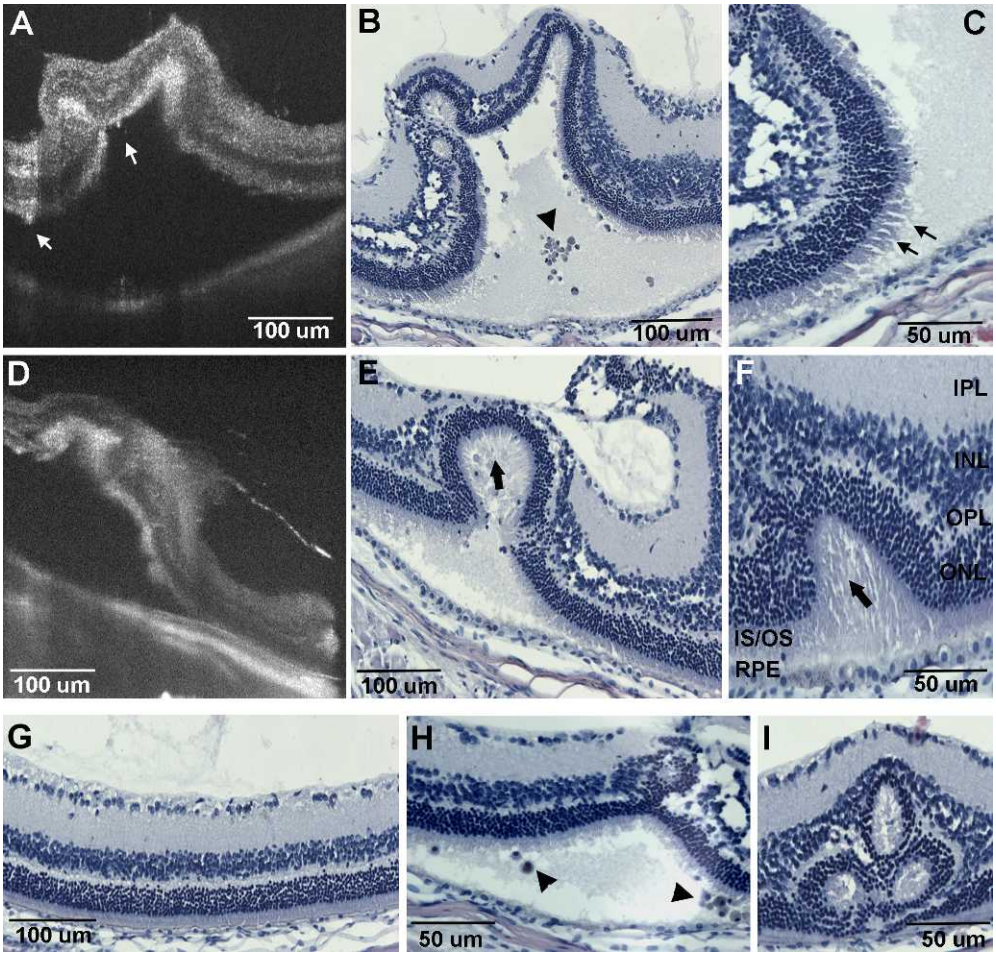

Figure 4. SD-OCT and light microscopic images of detached *Abca4*$^{-/-}$ mouse retina. SD-OCT (**A**, **D**) and H&E-stained histologic sections (**B**, **C**, **E**, **F**, **H**, **I**) of detached retina are shown. (**G**) Normal attached area of retina. (**A**, **D**) SD-OCT revealed rosette-like folds of neural retina with hyperreflectivity of the photoreceptor layer. The latter structures likely correspond to histologically visible folds and photoreceptor cell-rosettes. (**A**) *White arrows* denote hyperreflective material. (**B**, **H**) *Black arrowheads* indicate cells in the subretinal space. (**C**) *Thin black arrows* denote elongated photoreceptor outer segments. Partial (**F**, *thick black arrow*) and fully (**I**) developed rosettes.

on-spot emission maxima in the RD-*Abca4*$^{-/-}$ mouse retina was similar to the wavelength maxima reported previously for whole RPE lipofuscin.[26–28] Moreover, the spectrum acquired with the RD-*Abca4*$^{-/-}$ mouse retina exhibited a red-shift in emission maxima when excited at the longer wavelength (488 vs. 561 nm). Similar emission red-shifts with increasing excitation wavelengths have been observed for fundus autofluorescence[29] and RPE lipofuscin.[28] The fluorescence intensities of the "on-spot" recordings always were appreciably greater than the fluorescence intensities of the "off-spot" recordings.

Discussion

In the presence of a RD, loss of apposition between neural retina and RPE prevents RPE cells from phagocytosing the outer segment membrane, the result being that the shed photoreceptor outer segment material accumulates in the subretinal space.[17,30] With fundus AF imaging of detached mouse retina, we observed multiple intensely hyper-autofluorescent spots that were limited to areas of the detachment. These fluorescent puncta also were detected in flat-mounted retina viewed microscopically. The emission spectra recorded from these fluorescent spots were consistent with an origin from the bisretinoid fluorophores that form in photoreceptor cell outer segments and become the constituents of RPE lipofuscin. Moreover, images obtained by SD-OCT and light microscopy demonstrated that the hyper-autofluorescent spots in the detached retina likely corresponded to histologically visible clusters of photoreceptor cells arranged in rosettes, with outer segments oriented inwards. In SD-OCT images these rosette-like structures exhibited hyperreflective centers that probably corresponded to the outer segment-packed cores of these structures. The rosettes were approximately 192 × 156 μm and, thus, similar in size to the autofluorescent spots (diameter 185 μm) observed with fundus AF imaging. Taken together these observations indicated that the autofluorescence emitted from spots that decorate the area of detached retina stems from photoreceptor outer segments.

It has been established that the bisretinoid precursors that constitute RPE lipofuscin originate in photoreceptor outer segments.[31] For instance, bisretinoid precursors have been identified in outer segments isolated from bovine retina and *Abca4*$^{-/-}$ mice,[31,32] and by chromatography analysis it has been established that fluorophores that are similar spectroscopically to the bisretinoids of retina[18,33] accumulate in the degenerating photoreceptor outer segment debris in Royal College of Surgeons rats,[31,34] a strain having an inability to phagocytose shed outer segment membrane.[35,36] The amount

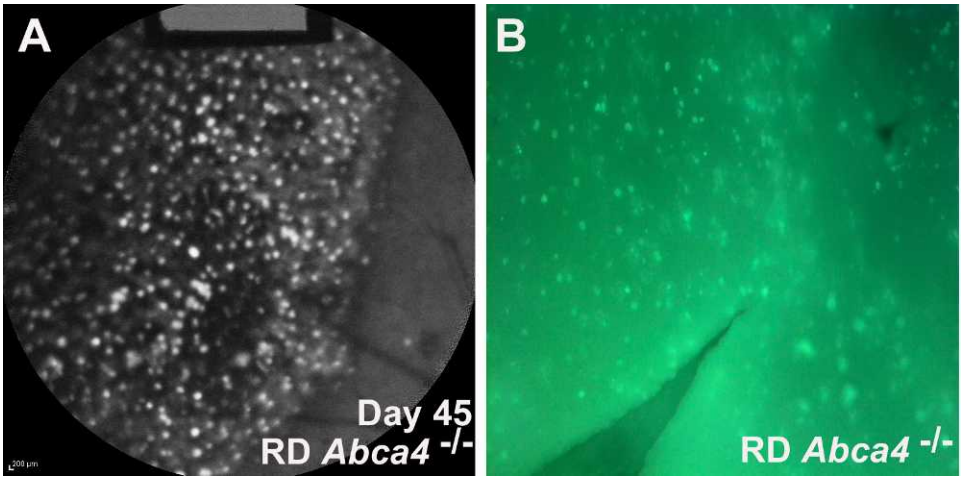

Figure 5. RD of *Abca4*$^{-/-}$ mice exhibits hyperfluorescent spots in in vivo fundus AF images that also are visible in fluorescence microscopic images ex vivo. (**A**) Fundus AF image of *Abca4*$^{-/-}$ mice (45 days post-detachment). (**B**) Representative fluorescence microscopic image of flat-mounted *Abca4*$^{-/-}$ retina. Note puncta of intense autofluorescence within the detachment retina (**A**, **B**).

of bisretinoid in healthy photoreceptor cells normally is not sufficient to make an appreciable contribution to fundus autofluorescence, since these compounds are transferred continuously to RPE cells through the process of outer segment shedding and RPE phagocytosis. We suggest, however, that this RD model serves as an example of a disorder in which photoreceptor cells become an aberrant source of fundus autofluorescence due to increased bisretinoid formation in impaired photoreceptor cells.[18] Since the fluorescence of retinal bisretinoids can be subject to photobleaching,[37,38] we suggested that this process could contribute to the gradual reduction in brightness observed for the autofluorescence puncta present in the area of detached retina.

RPE lipofuscin exhibits a peak emission of approximately 590–600 nm when excited by 488 nm light. In our present study, emission spectra recorded on the fluorescent spots exhibited fluorescence peaks at 581 and 629 nm, with excitations at 488 and 561 nm, respectively. The difference between the two excitation wavelengths was most noticeable with the on-spot versus off-spot recording. Specifically, the emission intensity generated with 488 nm excitation was considerable greater than with 561 nm excitation. The red-shift observed with the longer excitation wavelength is typical of fundus autofluorescence; individual retinal bisretinoids also exhibit a small but signature red-shift with longer excitation wavelength.[28] The formation of the hyper-autofluorescent spots was not restricted to *Abca4*$^{-/-}$ *mice,* which are notable for exhibiting an excessive accumulation of the bisretinoid pigments.[20,21,39] Wild-type mice also exhibited these changes within detached retina.

In our study, the combination of SD-OCT imaging, histology, and fluorescence spectroscopy aided our understanding of the origin of the hyperfluorescent spots observed in AF mode. Randomly distributed hyper-autofluorescent puncta, have been observed in some other mouse models of retinal degeneration.[40–42] Previous work exploring correlations between OCT

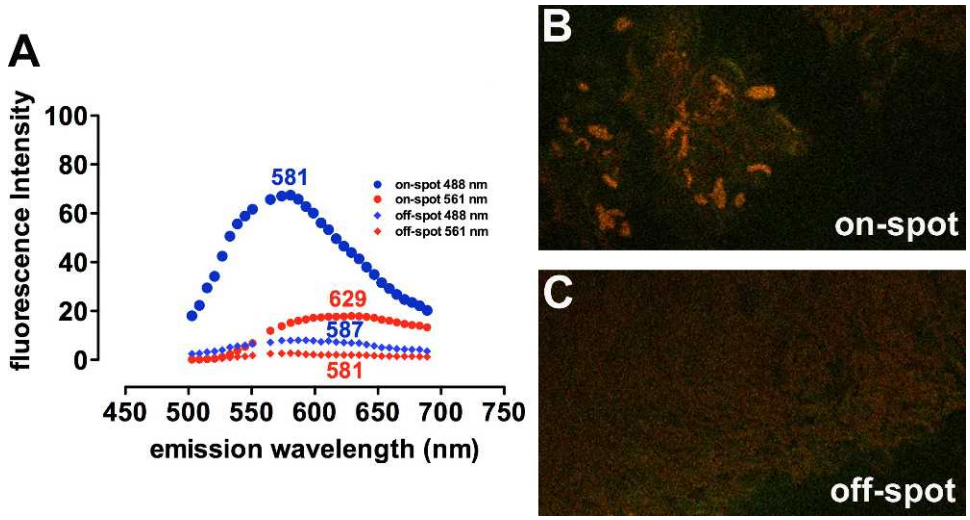

Figure 6. Fluorescence emission spectra and corresponding confocal microscopic images demonstrating recording areas on and off autofluorescent spots. (**A**) Fluorescence spectra obtained using flat-mounted *Abca4*$^{-/-}$ mouse retina in the presence of an RD. Data were recorded on spot (**B**; field size 512 × 512 pixels, 0.004 um per pixel) and off spot (**C**; field size 512 × 512 pixels, 0.010 um per pixel) using a confocal laser scanning fluorescence microscope 6 nm increments, and laser excitation at 488 and 561 nm as indicated. Emission data were adjusted for laser power. Peak emission wavelengths are indicated adjacent to each trace. Note red-shift with increasing excitation wavelength. The difference between the two excitation wavelengths is noticeable with the on-spot recording.

and histology in a mouse model of RD led to the suggestion that the hyperreflectivity seen in the photoreceptor layer[2] was caused by rearrangement and misalignment of the photoreceptors. Rosette-like formations within the degenerating retina of animal models of RD also have been reported.[3,43] Moreover, in the *Ccl2/Cx3cr1*-deficient mouse, histologically observed focal lesions within the photoreceptor cell layer were found to colocalize with hyperfluorescent regions detected in the fundus and with abnormal SD-OCT reflectance in the ONL.[44] However, the molecular source of the fluorescence was not discussed. In *rd7* mutant mice, retinal rosettes in histologic preparations were considered to correspond to white spots on color fundus photographs, but fundus AF imaging was not performed.[45] In other work characterizing *rd7* (*Nr2e3*^{rd7}) mice, investigators observed white spots in color fundus photographs, autofluorescence spots in whole-mounted retina and retinal folds in DAPI-stained histologic sections, and concluded that macrophages within the subretinal space were the source of the hyperautofluorescence.[42] Macrophage recruitment into the subretinal space is well documented,[1,46] but the origin and prevalence of subretinal phagocytes under conditions of RD is not clear. In the rabbit, it is supposed that the migration of RPE cells into the subretinal space serves as the major source of subretinal phagocytes.[47] In this scenario, RPE cells would be expected to migrate away from their monolayer and congregate close to the distal tips of the degenerating outer segments where they would phagocytose outer segment material. In our H&E histologic sections, the subretinal space contained a few melanin pigment-filled cells that could have originated from the RPE monolayer. These nuclei also could be attributed to immune cell recruitment.[2,3,46] Some nuclei in the subretinal space appeared pyknotic and could belong to apoptotic photoreceptor cells that have become displaced subretinally (photoreceptor drop-down).[23,48,49] In our experiments, macrophages could have accounted for fluorescent spot size and distribution in fundus AF images only if relatively large aggregates of these cells were situated at frequent intervals throughout the detached retina. We did not observe this phenomenon. Instead we noted photoreceptor cells rearranged in folds and within rosette-like structures along with elongated photoreceptor outer segments that more likely are the source of the AF spots. Many seemingly disparate diseases are associated with accumulations of autofluorescent material in the outer retina and/or in the subretinal space.[50] In our current study, we set out to contribute to the elucidation of hyper-autofluorescent puncta that are found commonly in cases of RD, including induced retinal disorders caused by physical separation of the photoreceptor outer segments from the RPE. Such is the case in central serous chorioretinopathy.[38] Efforts to clarify the source and aberrations of fundus hyper-autofluorescence are essential given the widespread use of fundus AF imaging in the diagnosis of many retinal disorders, along with plans for its use in monitoring treatment efficacy.

Acknowledgments

Katerine Wert and Janice David provided histologic preparations, and Joseph E. Vance of Bioptigen contributed to the study.

References

1. Anderson DH, Stern WH, Fisher SK, Erickson PA, Borgula GA. Retinal detachment in the cat: the pigment epithelial-photoreceptor interface. *Invest Ophthalmol Vis Sci*. 1983; 24:906–926.
2. Cebulla CM, Ruggeri M, Murray TG, Feuer WJ, Hernandez E. Spectral domain optical coherence tomography in a murine retinal detachment model. *Exp Eye Res*. 2010;90:521–527.
3. Chen HJ, Ma ZZ. N-Cadherin expression in a rat model of retinal detachment and reattachment. *Invest Ophthalmol Vis Sci*. 2007;48:1832–1838.
4. Li Q, Timmers AM, Hunter K, et al. Noninvasive imaging by optical coherence tomography to monitor retinal degeneration in the mouse. *Invest Ophthalmol Vis Sci*. 2001;42:2981–2989.
5. Nakanishi H, Hangai M, Unoki N, et al. Spectral-domain optical coherence tomography imaging of the detached macula in rhegmatogenous retinal detachment. *Retina*. 2009;29:232–242.
6. Wakabayashi T, Oshima Y, Fujimoto H, et al. Foveal microstructure and visual acuity after retinal detachment repair: imaging analysis by Fourier-domain optical coherence tomography. *Ophthalmology*. 2009;116:519–528.
7. Delori FC, Dorey CK, Staurenghi G, Arend O, Goger DG, Weiter JJ. In vivo fluorescence of the ocular fundus exhibits retinal pigment epithelium lipofuscin characteristics. *Invest Ophthalmol Vis Sci*. 1995;36:718–729.
8. Sparrow JR, Hicks D, Hamel CP. The retinal pigment epithelium in health and disease. *Curr Mol Med*. 2010;10: 802–823.
9. Lois N, Holder GE, Bunce C, Fitzke FW, Bird AC. Phenotypic subtypes of Stargardt macular dystrophy-fundus flavimaculatus. *Arch Ophthalmol*. 2001;119:359–369.
10. Vasireddy V, Jablonski MM, Khan NW, et al. Elovl4 5-bp deletion knock-in mouse model for Stargardt-like macular degeneration demonstrates accumulation of ELOVL4 and lipofuscin. *Exp Eye Res*. 2009;89:905–912.
11. von Ruckmann A, Fitzke FW, Bird AC. In vivo fundus autofluorescence in macular dystrophies. *Arch Ophthalmol*. 1997;115:609–615.
12. Holz FG, Bellman C, Staudt S, Schütt F, Volcker HE. Fundus autofluorescence and development of geographic atrophy in age-related macular degeneration. *Invest Ophthalmol Vis Sci*. 2001;42:1051–1056.
13. Holz FG, Bellmann C, Margaritidis M, Schütt F, Otto TP, Völcker HE. Patterns of increased in vivo fundus autofluorescence in the junctional zone of geographic atrophy of the retinal pigment epithelium associated with age-related macular degeneration. *Graefes Arch Clin Exp Ophthalmol*. 1999;237: 145–152.
14. Holz FG, Fleckenstein M, Schmitz-Valckenberg S, Bird AC. Evaluation of fundus autofluorescence images. In: Holz FG, Schmitz-Valckenberg S, Spaide RF, Bird AC, eds. *Atlas of Fundus Autofluorescence Imaging*. Berlin: Springer-Verlag; 2007:71–76.
15. Eandi CM, Ober M, Iranmanesh R, Peiretti E, Yannuzzi LA. Acute central serous chorioretinopathy and fundus autofluorescence. *Retina*. 2005;25:989–993.
16. Matsumoto H, Kishi S, Sato T, Mukai R. Fundus autofluorescence of elongated photoreceptor outer segments in central serous chorioretinopathy. *Am J Ophthalmol*. 2011;151:617–623.
17. Spaide RF, Klancnik JM Jr. Fundus autofluorescence and central serous chorioretinopathy. *Ophthalmology*. 2005;112: 825–833.
18. Sparrow JR, Yoon KD, Wu Y, Yamamoto K. Interpretations of fundus autofluorescence from studies of the bisretinoids of the retina. *Invest Ophthalmol Vis Sci*. 2010;51:4351–4357.
19. Delori F, Greenberg JP, Woods RL, et al. Quantitative measurements of autofluorescence with the scanning laser ophthalmoscope. *Invest Ophthalmol Vis Sci*. 2011;52:9379–9390.
20. Kim SR, Fishkin N, Kong J, Nakanishi K, Allikmets R, Sparrow JR. Rpe65 Leu450Met variant is associated with reduced levels of the retinal pigment epithelium lipofuscin fluorophores A2E and iso-A2E. *Proc Natl Acad Sci U S A*. 2004;101:11668–11672.
21. Weng J, Mata NL, Azarian SM, Tzekov RT, Birch DG, Travis GH. Insights into the function of Rim protein in photoreceptors

and etiology of Stargardt's disease from the phenotype in abcr knockout mice. *Cell*. 1999;98:13–23.

22. Wu Y, Fishkin NE, Pande A, Pande J, Sparrow JR. Novel lipofuscin bisretinoids prominent in human retina and in a model of recessive Stargardt disease. *J Biol Chem*. 2009;284: 20155–20166.
23. Zacks DN, Hanninen V, Pantcheva M, Ezra E, Grosskreutz C, Miller JW. Caspase activation in an experimental model of retinal detachment. *Invest Ophthalmol Vis Sci*. 2003;44:1262–1267.
24. Curcio CA, Messinger JD, Sloan KR, Mitra A, McGwin G, Spaide RF. Human chorioretinal layer thicknesses measured in macula-wide, high-resolution histologic sections. *Invest Ophthalmol Vis Sci*. 2011;52:3943–3954.
25. Spaide RF, Curcio CA. Anatomical correlates to the bands seen in the outer retina by optical coherence tomography: literature review and model. *Retina*. 2011;31:1609–1619.
26. Eldred GE, Katz ML. The autofluorescent products of lipid peroxidation may not be lipofuscin-like. *Free Radic Biol Med*. 1989;7:157–163.
27. Eldred GE, Miller GV, Stark WS, Feeney-Burns L. Lipofuscin: resolution of discrepant fluorescence data. *Science*. 1982;216: 757–759.
28. Sparrow JR, Wu Y, Nagasaki T, Yoon KD, Yamamoto K, Zhou J. Fundus autofluorescence and the bisretinoids of retina. *Photochem Photobiol Sci*. 2010;9:1480–1489.
29. Delori FC, Keilhauer C, Sparrow JR, Staurenghi G. Origin of fundus autofluorescence. In: Holz FG, Schmitz-Valckenberg S, Spaide RF, Bird AC, eds. *Atlas of Fundus Autofluorescence Imaging*. Berlin: Springer-Verlag; 2007:17–29.
30. Spaide RF, Noble K, Morgan A, Freund KB. Vitelliform macular dystrophy. *Ophthalmology*. 2006;113:1392–1400.
31. Ben-Shabat S, Parish CA, Vollmer HR, et al. Biosynthetic studies of A2E, a major fluorophore of retinal pigment epithelial lipofuscin. *J Biol Chem*. 2002;277:7183–7190.
32. Mata NL, Weng J, Travis GH. Biosynthesis of a major lipofuscin fluorophore in mice and humans with ABCR-mediated retinal and macular degeneration. *Proc Natl Acad Sci U S A*. 2000;97: 7154–7159.
33. Sparrow JR, Parish CA, Hashimoto M, Nakanishi K. A2E, a lipofuscin fluorophore, in human retinal pigmented epithelial cells in culture. *Invest Ophthalmol Vis Sci*. 1999;40:2988–2995.
34. Katz ML, Eldred GE, Robison WG Jr. Lipofuscin autofluorescence: evidence for vitamin A involvement in the retina. *Mech Ageing Dev*. 1987;39:81–90.
35. Edwards RB, Szamier RB. Defective phagocytosis of isolated rod outer segments by RCS rat retinal pigment epithelium in culture. *Science*. 1977;197:1001–1003.
36. Matthes MT, LaVail MM. Inherited retinal dystrophy in the RCS rat: composition of the outer segment debris zone. *Prog Clin Biol Res*. 1989;314:315–330.
37. Hunter JJ, Morgan JI, Merigan WH, Sliney DH, Sparrow JR, Williams DR. The susceptibility of the retina to photochemical damage from visible light. *Prog Retin Eye Res*. 2012;31:28–42.
38. Yamamoto K, Zhou J, Hunter JJ, Williams DR, Sparrow JR. Toward an understanding of bisretinoid autofluorescence bleaching and recovery. *Invest Ophthalmol Vis Sci*. 2012;53: 3536–3544.
39. Kim SR, Jang YP, Jockusch S, Fishkin NE, Turro NJ, Sparrow JR. The all-trans-retinal dimer series of lipofuscin pigments in retinal pigment epithelial cells in a recessive Stargardt disease model. *Proc Natl Acad Sci U S A*. 2007;104:19273–19278.
40. Huber G, Beck SC, Grimm C, et al. Spectral domain optical coherence tomography in mouse models of retinal degeneration. *Invest Ophthalmol Vis Sci*. 2009;50:5888–5895.
41. Seeliger MW, Beck SC, Pereyra-Munoz N, et al. In vivo confocal imaging of the retina in animal models using scanning laser ophthalmoscopy. *Vision Res*. 2005;45:3512–3519.
42. Wang NK. Fine HF, Chang S, et al. Cellular origin of fundus autofluorescence in patients and mice with a defective NR2E3 gene. *Br J Ophthalmol*. 2009;93:1234–1240.
43. Maeda A, Maeda T, Golczak M, Palczewski K. Retinopathy in mice induced by disrupted all-trans-retinal clearance. *J Biol Chem*. 2008;283:26684–26693.
44. Zhou YD, Sheets KG, Knott EJ, et al. Cellular and 3D optical coherence tomography assessment during the initiation and progression of retinal degeneration in the Ccl2/Cx3cr1-deficient mouse. *Exp Eye Res*. 2011;93:636–648.
45. Akhmedov NB, Piriev NI, Chang B, et al. A deletion in a photoreceptor-specific nuclear receptor mRNA causes retinal degeneration in the rd7 mouse. *Proc Natl Acad Sci U S A*. 2000;97:5551–5556.
46. Hisatomi T, Sakamoto T, Sonoda KH, et al. Clearance of apoptotic photoreceptors: elimination of apoptotic debris into the subretinal space and macrophage-mediated phagocytosis via phosphatidylserine receptor and integrin alphavbeta3. *Am J Pathol*. 2003;162:1869–1879.
47. Johnson NF, Foulds WS. Observations on the retinal pigment epithelium and retinal macrophages in experimental retinal detachment. *Br J Ophthalmol*. 1977;61:564–572.
48. Arroyo JG, Yang L, Bula D, Chen DF. Photoreceptor apoptosis in human retinal detachment. *Am J Ophthalmol*. 2005;139: 605–610.
49. Chang CJ, Lai WW, Edward DP, Tso MO. Apoptotic photoreceptor cell death after traumatic retinal detachment in humans. *Arch Ophthalmol*. 1995;113:880–886.
50. Spaide R. Autofluorescence from the outer retina and subretinal space: hypothesis and review. *Retina*. 2008;28:5–35.